Available online at www.sciencedirect.com
ScienceDirect
Trans. Nonferrous Met. Soc. China 20(2010) 71−77
Transactions of Nonferrous Metals Society of China
www.tnmsc.cn

Correlation between microstructure and thermal dilation behavior of amorphous Fe-Co-Zr-Mo-W-B alloys

ZHANG Ji-teng(张集滕)[1], WANG Wei-min(王伟民)[1,2], LI Gui-hua(李桂华)[1], MA Hai-jian(马海健)[1], QIN Jing-yu(秦敬玉)[1], BIAN Xiu-fang(边秀房)[1]

1. Key Laboratory for Liquid-Solid Structural Evolution and Processing of Materials, Ministry of Education, Shandong University, Ji'nan 250061, China;
2. Key Laboratory of Metastable Materials Science and Technology, Yanshan University, Qinhuangdao 066004, China

Received 9 December 2008; accepted 7 April 2009

Abstract: The microstructures and thermal properties of $Fe_{61}Co_{9-x}Zr_8Mo_5W_xB_{17}$ (x=0 and 2) formed under different vacuum conditions were investigated by scanning electron microscopy(SEM), X-ray diffractometry(XRD), transmission electron microscopy(TEM), and conventional dilatometry(DIL). The variation of the non-monotonic effects of tungsten content and vacuum conditions on the glass forming ability(GFA) of Fe-based alloys can be drawn in a schematic diagram. The higher the GFA of alloys, the higher the difference between the thermal expansion coefficients of glassy state and crystalline state($\Delta\alpha$), which can be described by the free volume model during dilatometric measurements. Under low and high vacuum conditions, the viscosity and microhardness are improved and the fragility of the Fe-based alloys are decreased by adding tungsten.
Key words: glass forming ability; viscosity; fragility; Fe-based alloys

1 Introduction

Bulk metallic glasses(BMGs) such as Mg-, Ln-, Zr-, Cu- and Fe-based systems have been drawing increasing attention in recent years due to their interesting properties[1−3]. As a member of the family of BMG systems, Fe-based alloys are commercially the most important not only due to much cheaper than other BMGs, but also due to the unique combination of high physical, chemical and mechanical properties[4−5]. Since INOUE et al[6] synthesized Fe-Co-(Zr, Nb, Ta)-(Mo, W)-B amorphous alloys in 1997, a lot of work has been done on this system, especially on the $Fe_{61}Co_7Zr_{10}Mo_5W_2B_{15}$ alloy[7] because of its high glass forming ability(GFA), high thermal stability, high strength and high corrosion resistance.

Generally, BMGs have a tendency to unalterable structural relaxation, which can affect many of their properties, attributing to high cooling rates. Furthermore, different thermal expansion behaviors of BMGs are closely associated with their applications[8]. Consequently, it is quite important to investigate the thermal expansion behaviors of BMGs. Since the method of obtaining the values of viscosity from dilatation measurement was proposed, the viscosity has been widely calculated from the sample length changes[9]. The concept of fragility is defined as the increasing rate of the viscosity of a supercooled liquid at the glass transition temperature based on analysis of plots of logarithmic viscosity as a function of inverse temperature[10].

Oxygen plays an important role in the GFA, structure, thermal stability and other properties of the Fe-based alloys, because metal oxides can trigger nucleation of crystalline phases[11]. In order to analyze the effect of vacuum on the various properties of amorphous Fe-Co-Zr-Mo-W-B alloy, we pump the casting chamber to high vacuum (10^{-3} Pa) condition and low vacuum (10 Pa) condition. Subsequently, we investigate microstructure, thermal expansion coefficient, viscosity, fragility and microhardness of the $Fe_{61}Co_{9-x}$-

Foundation item: Projects(50871061, 50871062, 50631010, 50831003, 50801041) supported by the National Natural Science Foundation of China; Project (2008BS04020) supported by the Shandong Excellent Youthy Award Foundation, China; Project(NCET-06-584) supported by Ministry of Education of China; Project(2007CB613901) supported by the National Basic Research Program of China
Corresponding author: WANG Wei-min; Tel: +86-531-88392749; E-mail: weiminw@sdu.edu.cn
DOI: 10.1016/S1003-6326(09)60099-6

$Zr_8Mo_5W_xB_{17}$ (x=0 and 2) alloys.

2 Experimental

The $Fe_{61}Co_{9-x}Zr_8Mo_5W_xB_{17}$ (x=0 and 2) samples used in this work were obtained by induction-melting the mixture of pure metals, except that B was added using a Fe-16.8%B (mass fraction) master alloy. All ingots were re-molten at least three times to guarantee the homogeneity of each element. Bulk rods were obtained by injection casting into copper moulds of 2 mm in diameter and 50 mm in length under an argon atmosphere.

In order to analyze the effect of vacuum on the amorphous Fe-Co-Zr-Mo-B alloy, we reduced the pressure of the casting chamber to 2.0×10^{-3} Pa with the mechanical vacuum pump and molecular vacuum pump, then input 6×10^4 Pa argon before injection casting, labeled as condition VH. Furthermore, we reduced vacuum of the casting chamber to 20 Pa with the mechanical vacuum pump only, and then input 6×10^4 Pa argon before injection casting, labeled as condition VL. The oxygen contents(w(O)) of these samples were measured using a C436 LECO analyzer. It is found that, in the case of x=0, w(O) values for the rod with VH and VL are 0.007 7% and 0.003 0% (mass fraction) respectively; and in the case of x=2, w(O) values for the rod with VH and VL are 0.004 0% and 0.003 3% (mass fraction), respectively.

The phases in these samples were investigated by X-ray diffraction(XRD) using a PHILIP PW 3020 diffractometer with Co K_α radiation (λ=0.178 89 nm). The microstructure and local compositions of these samples were investigated by scanning electron microscope (SEM, S−2500 and JEOL−JSM−6400), transmission electron microscope (TEM, H−800), and metallographic microscope (KH−2200). The Vickers hardness was averaged from 8 tests, with a HVS−1000 microhardness tester at room temperature under a load of 9.8 N and a holding time of 10 s.

The dilatation measurements were conducted with a conventional dilatometer (Netzsch DIL 402C) at a heating rate of 10 K/min. The dilation measurement, as described by VLASAK et al[9], was applied to measuring the viscosity of glassy alloys. In this method, the overall length changes, Δl, may be written as

$$\Delta l(t,T,\sigma)=l_0\int_{T_0}^{T}\alpha(T)\mathrm{d}T+l_0\sigma\int_{T_0}^{T}\frac{\alpha(T)}{E(T)}\mathrm{d}T+ l(T)K\sigma\int_0^{t(T)}\frac{1}{\eta(T)}\mathrm{d}t \quad (1)$$

where l_0 is the length of the sample at the temperature of T_0; $\alpha(T)$ is the thermal dilatation coefficient of the sample; $E(T)$ is the elastic modulus; $l(T)$ is the length of the sample at the temperature of T; σ is the applied load; K is a numerical constant; and $\eta(T)$ is the viscosity of the sample. The first term is the thermal dilatation of the sample, which is generally supposed to be very similar to that of the crystallized sample. The second term is obtained by the elasticity under applied specific load σ, and the contribution of this term in these alloys to overall length changes is small enough to be negligible. Obviously, the last term reflects the flow of the sample under applied load.

For simplification, the thermal dilation coefficient of the amorphous sample is considered similar to that of its crystal and the elastic elongation is neglected. So, the viscosity may be expressed as[9]

$$\eta(T)=\frac{Kl_{\mathrm{sub}}(T)\sigma}{\mathrm{d}\Delta l_{\mathrm{sub}}(T)/\mathrm{d}t}=\frac{Kl_{\mathrm{sub}}(T)\sigma}{(\mathrm{d}\Delta l_{\mathrm{sub}}(T)/\mathrm{d}t)(\mathrm{d}T/\mathrm{d}t)} \quad (2)$$

where $\Delta l_{\mathrm{sub}}=\Delta l-l_0\int_{T_0}^{T}\alpha(T)\mathrm{d}T$; and $l_{\mathrm{sub}}=l-l_0\int_{T_0}^{T}\alpha(T)\mathrm{d}T$. Therefore, the viscosity of the sample can be calculated using Eq.(2) when the viscosity is supposed to be 10^{12} Pa·s at T_g[10].

3 Results

3.1 Microstructure and GFA of amorphous Fe-based alloys

Fig.1 shows the SEM micrographs of $Fe_{61}Co_{9-x}Zr_8Mo_5W_xB_{17}$ (x=0 and 2) rods under different vacuum conditions, together with the corresponding XRD patterns. In the rod with x=0 and VH, there exist a number of precipitates of 1−2 μm in diameter embedded in the amorphous matrix, and EDAX shows the bright central part of the precipitate is Zr-rich, while the dark outside part is Fe-rich (Fig.1(a) and bottom-right inset). The XRD pattern displays a typical amorphous halo together with the crystalline peaks, which are identified as α-Fe, Fe_2B, $Fe_{23}Zr_6$ and Fe_8B phases (top-right inset of Fig.1(a)). In the rod with x=0 and VL, no obvious precipitate can be found in the amorphous matrix (Fig.1(b)), which is consistent with its XRD pattern (top-right inset of Fig.1(b)). In the rod with x=2 and VH, there is also no obvious precipitated phase in the SEM micrographs and XRD pattern (Fig.1(c) and top-right inset). However, in the rod with x=2 and VL, the dark dendritic precipitates appear in the amorphous matrix, and the width and length of the precipitates are about 2 μm and 5−10 μm, respectively, which are obviously larger than the precipitates in the rod with x=0 and VH (Fig.1(d)); while the number of the precipitates is far lower than that in the rod with x=0 and VH (Fig.1(a)). EDAX analysis verifies that the precipitates are Zr-rich

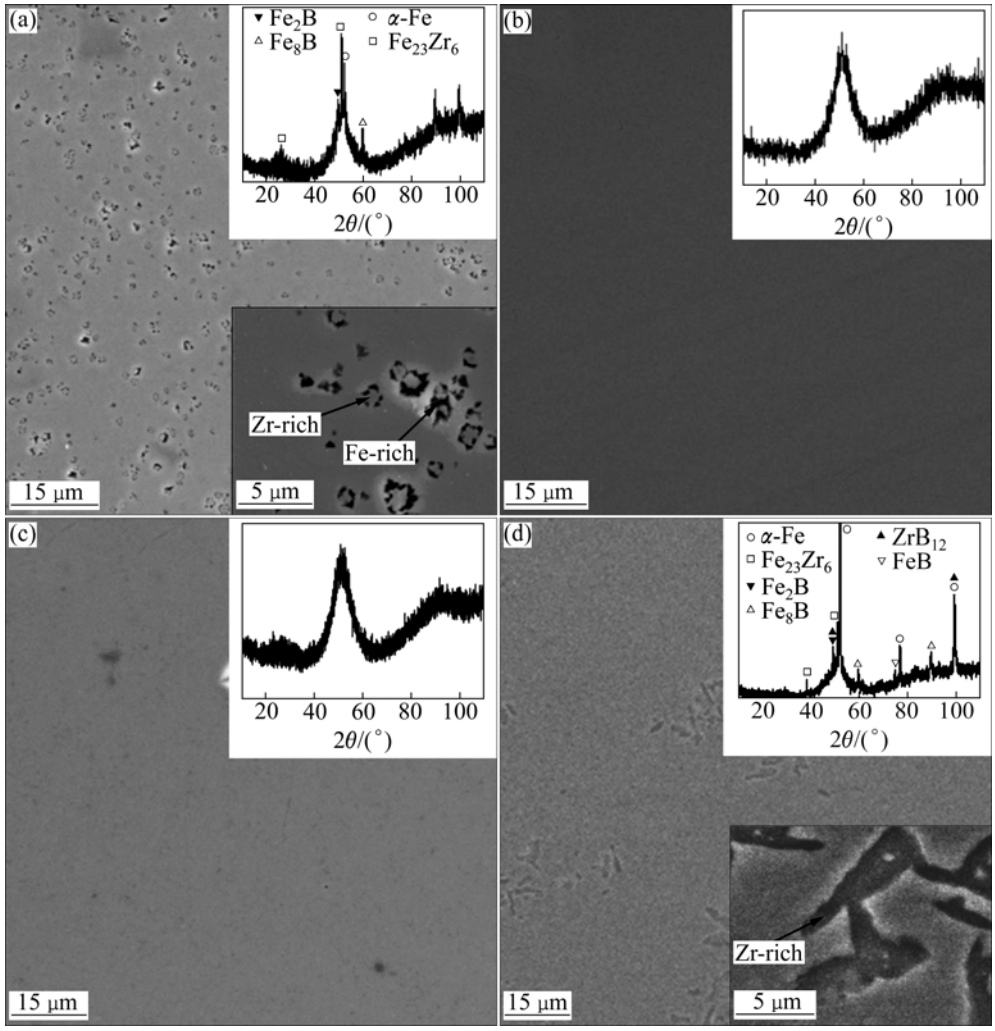

Fig.1 SEM micrographs of as-cast $Fe_{61}Co_{9-x}Zr_8Mo_5W_xB_{17}$ rods with different conditions: (a) x=0, VH; (b) x=0, VL; (c) x=2, VH; (d) x=2, VL (Top-right insets give corresponding XRD patterns, and bottom-right insets present magnification of precipitates in corresponding rods)

(bottom-right inset of Fig.1(d)). The XRD pattern exhibits a typical glassy maximum as well as the crystalline peaks, which are identified as α-Fe, $Fe_{23}Zr_6$, ZrB_{12}, Fe_2B, Fe_8B, and FeB phases (top-right inset of Fig.1(d)).

These results suggest that, in the case of x=0, low vacuum is helpful for improving the glass forming ability (GFA) of the alloy, which is supported by the GFA parameter γ of 0.390 and 0.395 for the conditions VH and VL, respectively. The results also suggest that, in the case of x=2, low vacuum is harmful for the GFA, which is consistent with the γ values of 0.396 and 0.386 for the conditions VH and VL, respectively.

In order to confirm the type of the precipitates in the rod with x=0 and VH as well as the rod with x=2 and VL, their bright field TEM micrographs and selected area electron diffraction(SAED) patterns are shown in Fig.2. In the rod with x=0 and VH, the rose-like precipitate is of about 0.5 μm in diameter, consisting of other phases outside (Fig.2(a)). The phases can be identified by SAED as $Fe_{23}Zr_6$ and Fe_2B (Fig.2(b)), which are consistent with XRD pattern (top-right inset of Fig.1(a)). Meanwhile, the width and length of the arm of star-like precipitate are 0.1 μm and 0.7 μm (Fig.2(c)), respectively, which exhibits a similar ratio to that of the precipitate in the corresponding SEM micrograph (Fig.1(d)). The SAED patterns show that the type of precipitate is ZrB_{12} and the orientation of one arm is different from the other (Fig.2(d)). Similarly, the type of the precipitate is consistent with the XRD pattern (top-right inset of Fig.1(d)).

3.2 Thermal expansion behaviors of amorphous Fe-based alloys

Fig.3 shows the thermal expansion curves of the $Fe_{61}Co_{9-x}Zr_8Mo_5W_xB_{17}$ (x=0 and 2) rods with various vacuum conditions. The four rods exhibit a similar thermal expansion behavior, which can be divided into

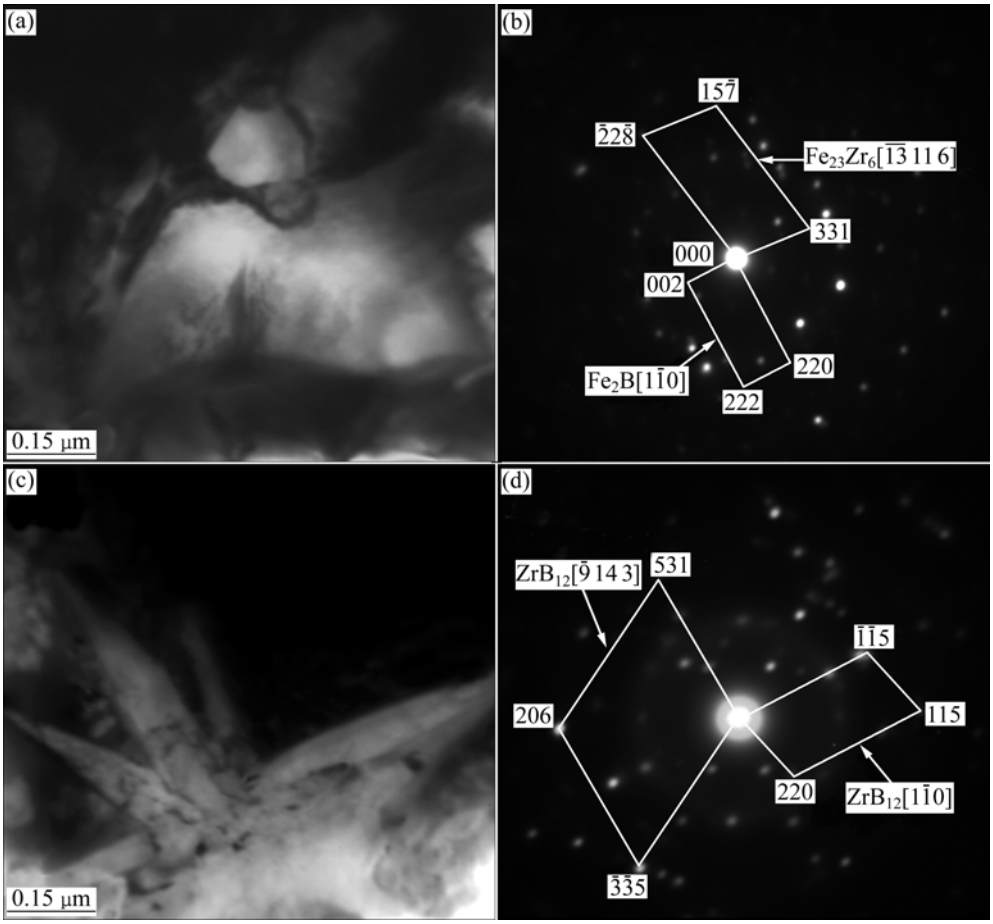

Fig.2 Bright field TEM images and selected area diffraction patterns of as-cast $Fe_{61}Co_{9-x}Zr_8Mo_5W_xB_{17}$ rods under different conditions: (a), (b) x=0, VH; (c), (d) x=2, VL

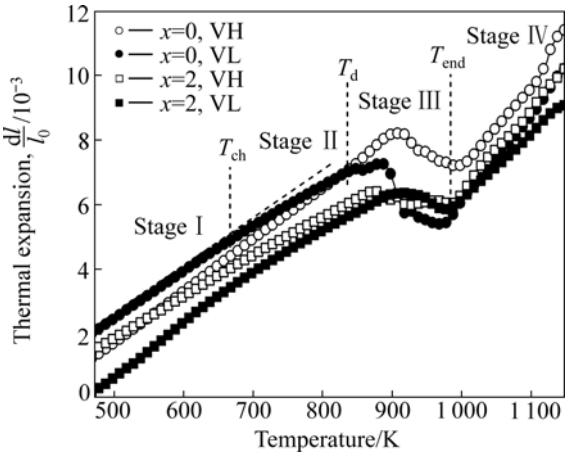

Fig.3 Thermal expansion curves of $Fe_{61}Co_{9-x}Zr_8Mo_5W_xB_{17}$ (x= 0 and 2) rods with different vacuum conditions at heating rate of 10 K/min

four stages:

1) Stage Ⅰ: the thermal expansion curves of four rods exhibit a linear shape until about 660 K, denoted by T_{ch} in Fig.3.

2) Stage Ⅱ: from T_{ch} to the temperature when the samples lengths start to decrease, denoted by T_d in Fig.3, the thermal expansion curves are still in linear shape with lower slopes than those in stage Ⅰ since T_{ch} is much lower than the glass transition temperatures (T_g) of the rods. The slope change can be ascribed to the structural relaxation of the glassy alloy[12].

3) Stage Ⅲ: from T_d to the end of the decrease procedure of sample length, denoted by T_{end} in Fig.3, the expansion curves exhibit differently. The contraction results from the viscous flow of the alloy in the supercooled liquid state under the action of the compression load for length measurement as well as the crystallization processes[13].

4) Stage Ⅳ: above T_{end}, the thermal expansion curves turn back to be linear, suggesting that the rods are in full crystalline state.

The average glassy expansion coefficient, α_g, can be obtained in the first linear part of the expansion curves (stage Ⅰ in Fig.3). And the average crystalline expansion coefficient, α_c, can be obtained in the last linear part of the expansion curves (stage Ⅳ in Fig.3). The expansion coefficient difference, $\Delta\alpha=\alpha_c-\alpha_g$, between stage Ⅰ and stage Ⅳ, can be obtained. For clarification, Table 1 lists the thermal parameters such as glass transition temperature T_g and onset of first crystallization T_x, and the dilatometric parameters such as the average glassy

Table 1 Thermal and dilatation parameters of $Fe_{61}Co_{9-x}Zr_8Mo_5W_xB_{17}$ (x=0 and 2) rods with different vacuum conditions

Sample condition	T_g/K	T_x/K	T_{ch}/K	T_d/K	T_{end}/K	γ	$\alpha_g/10^{-6}\,K^{-1}$	$\alpha_c/10^{-6}\,K^{-1}$	$\Delta\alpha/10^{-6}\,K^{-1}$
x=0, VH	846[14]	916[14]	590	907	1 005	0.390	15.8	25.04	9.24
x=0, VL	855	933	660	835	1 000	0.395	13.2	26.99	13.79
x=2, VH	870[14]	942[14]	680	877	987	0.396	12.1	26.02	13.92
x=2, VL	868	925	650	920	977	0.386	14.7	20.88	6.18

and crystalline expansion coefficients α_g and α_c together with their difference. As shown in Fig.3 and Table 1, in the case of x=0, the $\Delta\alpha$ of the rod with VH is lower than that of the rod with VL; meanwhile, in the case of x=2, the $\Delta\alpha$ of the rod with VH is higher than that of the rod with VL. Under the same condition of VH, the $\Delta\alpha$ of the rod with condition x=0 is lower than that of the rod with condition x=2; while under the same condition of VL, the $\Delta\alpha$ of the rod with condition x=0 is higher than that of the rod with condition x=2. In the case of x=0, the α_g of the rod with VH is higher than that of the rod with VL; meanwhile, in the case of x=2, the α_g of the rod with VH is lower than that of the rod with VL. It can be concluded that the α_g of the sample which contains crystals is higher than that of fully glassy sample.

3.3 Viscosity and microhardness of amorphous Fe-based alloy

Based on Eq.(2), the DIL viscosity of the glassy alloy can be calculated by the flow of the sample during the expansion measurement. Fig.4 shows the DIL viscosity of the $Fe_{61}Co_{9-x}Zr_8Mo_5W_xB_{17}$ (x=0 and 2) rods with various vacuum conditions in the supercooled liquid region. In the case of x=0, the DIL viscosity of the rod with condition VH is lower than that of the rod with condition VL in the temperature range of 850−873 K, while in the case of x=2, the DIL viscosity of the rod with condition VH is higher than that of the rod with condition VL. In the same condition of VH, the DIL viscosity of the rod with condition x=0 is lower than that of the rod with condition x=2, while in the same condition of VL, the DIL viscosity of the rod with condition x=0 is lower than that of the rod with condition x=2 in the temperature range of 850−928 K, showing that tungsten can increase the DIL viscosity of the sample.

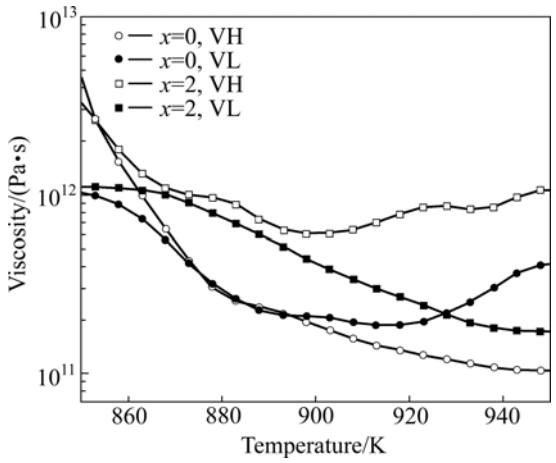

Fig.4 Viscosities of $Fe_{61}Co_{9-x}Zr_8Mo_5W_xB_{17}$ (x=0 and 2) samples with different vacuum conditions in supercooled liquid region

Fig.5 shows the microhardness of $Fe_{61}Co_{9-x}Zr_8Mo_5W_xB_{17}$ (x=0 and 2) rods with various vacuum conditions. The values of the rods with x=0 and 2 in the same condition VH are obtained in the Ref.[15]. In both conditions VH and VL, the microhardness of the rod with x=0 is lower than that of the rod with x=2. This shows that tungsten can increase the hardness of the sample. Based on the results of Figs.4 and 5, it can be concluded that the higher the DIL viscosity of the sample up to 873 K, the higher the microhardness of the sample with the same tungsten content.

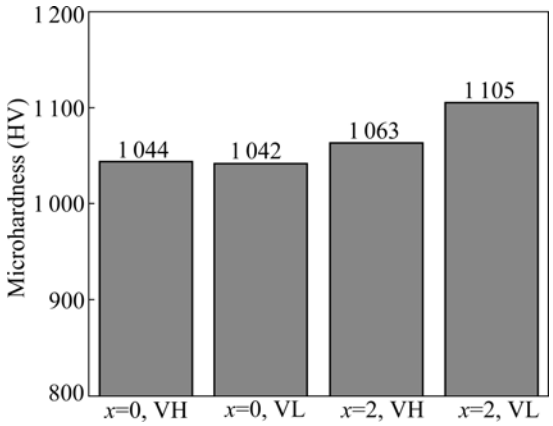

Fig.5 Microhardness of $Fe_{61}Co_{9-x}Zr_8Mo_5W_xB_{17}$ (x=0 and 2) rods with different vacuum conditions

4 Discussion

From Fig.1, the GFA of the alloy is dependent on tungsten content and vacuum condition. We consider that the vacuum is quantitatively associated to oxygen content in the system, and construct a pseudo-ternary phase diagram to explain the present results, as shown in Fig.6, which is stimulated by the earlier published typical ternary phase diagram[16]. Alloys A, B, C and D present the rods with x=0 and VL, x=2 and VL, x=2 and VH, x=0 and VH, respectively. Obviously, alloys A and C can be cast into almost fully amorphous rods, but alloys B and

D cannot. The solid arrows point from weak GFA to strong GFA in the phase diagram (Fig.6). Generally, the bulk metallic glasses are multi-component alloy phases with relatively narrow composition ranges[14]. In the ternary and pseudo-ternary phase diagrams, the BMG formation limit is often indicated by the ellipse or convex polygon zone[16−17]. Hence, the BMG limit can be drawn by the diagonal ellipse in Fig.6. It is clear that alloys D and B is outside the range of BMG formation limit, which helps us to understand their worse GFA compared with alloys A and C. From Table 1, we can find the sequences of T_x and $\Delta\alpha$ of the alloys are similar to those of GFA, shown by the dash and dot arrows respectively, in Fig.6. It is known that the metallic glass stays in an unstable state with some free volume frozen in it owing to the rapid cooling rate. When the glass is heated, the free volume will be released, resulting in the contraction in the length. The more the amorphous phase in the sample, the more the free volume to be released[18]. Therefore, we can understand that the thermal expansion coefficient difference of the rods is consistent with the GFA, as shown in Fig.6. Furthermore, the higher the GFA of alloy is, the higher the thermal stability and the crystallization temperature T_x are[19], as described in Fig.6.

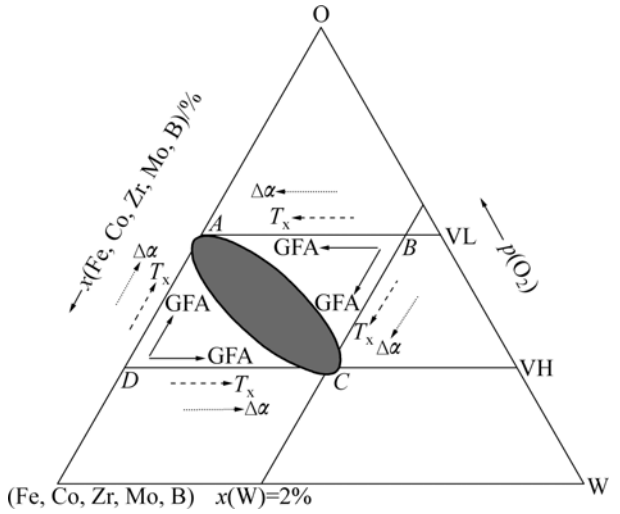

Fig.6 Schematic diagram of variation of measured parameters with tungsten content and oxygen pressure ($p(O_2)$) during casting

The viscosity of the glasses in the supper-cooled region is often described by the Vogel-Fulcher-Tammann equation[3]:

$$\ln\eta = \ln\eta_0 + \frac{DT_g^0}{(T - T_g^0)} \tag{3}$$

where η_0 equals h_p/V_m with Plank's constant h_p and the atomic/molecular volume V_m; T_g^0, the asymptotic value of T_g, is usually approximated as the onset of glass transition in the limit of infinitely slow cooling/heating rate; and D is the fragility parameter. Fig.7 shows the Angell plot including the DIL viscosities of $Fe_{61}Co_{9-x}Zr_8Mo_5W_xB_{17}$ (x=0 and 2) rods with various vacuum conditions which are fitted by VFT equation as well as SiO_2[10]. As is known to us, the fragility will be higher when the departure degree of the fitting line below SiO_2 line is higher in the vicinity of T_g/T=1. Here, in the case of x=0, the fragility of the rod with condition VH is higher than that of the rod with condition VL, while in the case of x=2, the fragility of the rod with condition VH is lower than that of the rod with condition VL. Based on Angell's viewpoint[10], it can be obtained that the lower the fragility of alloys, the higher the GFA of alloys because the lower fragility liquid behavior of BMG generally leads to the sluggish kinetics in the supercooled liquid region and nucleation and growth of crystals are suppressed. This agrees well with their GFA in the Figs.1 and 6. In addition, under condition VH, the fragility of the rod with x=0 is higher than that with x=2; under condition VL, however, the fragility of the rod with x = 0 is higher than that of with x=2, showing that tungsten can decrease the fragility of the sample.

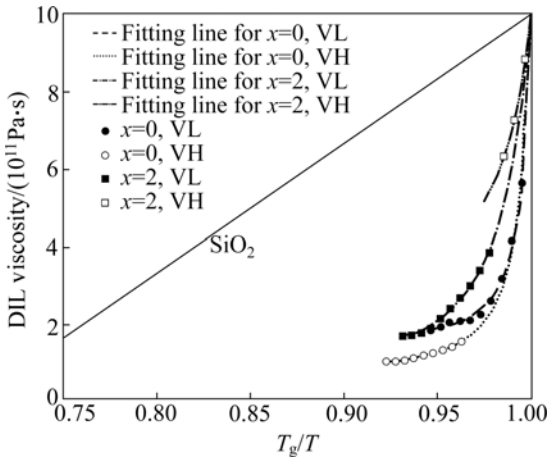

Fig.7 Angell plot including DIL viscosities of $Fe_{61}Co_{9-x}Zr_8Mo_5$- W_xB_{17} (x=0 and 2) rods with different vacuum conditions obtained by VFT equation, together with strong glass of SiO_2 [12] (T_g^* is temperature at which viscosity is 10^{12} Pa·s)

In Fig.1(a), it is clear that there exist a number of precipitates of 1−2 μm in diameter embedded in the amorphous matrix of the rod with x=0 and VH; however, no obvious precipitates appear in the rod with x=0 and VL in Fig.1(b). Based on the fact that the viscosity of the rod with x=0 and VH is lower than that of the rod with x=0 and VL in the supercooled liquid region shown in Fig.4, we can deduce that the viscosity of the supercooled melt with VH before quenching will be further lower than that with VL, according to Ref.[20].

Hence, it will be easier for the Zr and Fe atoms in the supercooled melt with VH to diffuse, and $Fe_{23}Zr_6$ phases can be easily participated out (Fig.1(a)). Obviously, the oxygen in the atmosphere improves the viscosity of the supercooled melt without tungsten addition. In the case of x=2, as shown in Figs.1(c) and (d), no obvious precipitates appear in the rod with VH while a number of dark dendritic precipitates appear in the rod with VL. As the viscosity of the rod with VH is higher than that of the rod with VL in the supercooled liquid region in Fig.4, the supercooled melt with VH before quenching will be further higher than that with VL[20]. Consequently, it will be easier for the atoms in the supercooled melt with VL to diffuse, and Zr-rich phases can be precipitated, as shown in Fig.1(d). Moreover, among the transition metals, the electronegativity of tungsten e(W)=2.36 is the secondly highest and rather close to 3.44 of oxygen[21], hence, tungsten might replace the oxygen to react with Fe and Zr atoms and possibly reach the saturated concentration with x=2 and VL. Therefore, the effect of the tungsten and oxygen contents on the viscosity can be explained, which is also displayed in Fig.6.

5 Conclusions

1) SEM and XRD results show the GFA of $Fe_{61}Co_{9-x}Zr_8Mo_5W_xB_{17}$ (x=0 and 2) alloys is dependent on the tungsten content and vacuum conditions, which can be described by a pseudo-ternary phase diagram.

2) The dilatometric measurement shows the higher the GFA, the higher the $\Delta\alpha$, which can be explained by the free volume model.

3) Under low and high vacuum conditions, tungsten can improve the viscosity and hardness, and decrease the fragility of the Fe-based alloys.

Acknowledgements

The authors acknowledge Dr. A. GEBERT, Prof. J. ECKERT and Prof. L. SCHULTZ in IFW-Dresden for technical supports. They also acknowledge the financial support from the Alexander-von-Humboldt Foundation, Germany.

References

[1] INOUE A, ZHANG T, NISHIYAMA N. Preparation of 16 mm diameter rod of amorphous $Zr_{65}Al_{7.5}Ni_{10}Cu_{17.5}$ alloy [J]. Mater Trans JIM, 1993, 34: 1234−1237.

[2] QIN C L, ZHANG W, ASAMI K, KIMURA H, WANG X M, INOUE A. A novel Cu-based BMG composite with high corrosion resistance and excellent mechanical properties [J]. Acta Mater, 2006, 54: 3713−3719.

[3] INOUE A, SHINOHARA Y, GOOK J S. Thermal and magnetic properties of bulk Fe-based alloys prepared by copper mold casting [J]. Mater Trans JIM, 1996, 37: 1427−1431.

[4] JOHNSON W L. Bulk amorphous metal—An emerging engineering material [J]. JOM, 2002, 54: 40−43.

[5] SHEN T D, SCHWARZ R B. Direct measurement of strain in a Ge island on Si [J]. Appl Phys Lett, 1999, 40: 1019.

[6] INOUE A, ZHANG T, TAKEUCHI A. Bulk amorphous alloys with high mechanical strength and good soft magnetic properties in Fe-TM-B (Ⅳ-Ⅷ group transition metal) system [J]. Appl Phys Lett, 1997, 71: 464.

[7] INOUE A. Bulk amorphous FC20 (Fe-C-Si) alloys with small amounts of B and their crystallized structure and mechanical properties [J]. Acta Mater, 2000, 48: 1383−1395.

[8] DAMASCHKE B, SAMWER K. Preparation of rare-earth manganite-oxide thin films by metal organic aerosol deposition technique [J]. Appl Phys Lett, 1999, 75: 1511.

[9] VLASAK G, SVEC P, DUHAJ P. Application of isochronal dilatation measurements for determination of viscosity of amorphous alloys [J]. Mater Sci Eng A, 2001, 472: 304−306.

[10] ANGELL C A. Formation of glasses from liquids and biopolymers [J]. Science, 1995, 267: 1924−1935.

[11] SHEN T D, SCHWARZ R B. Bulk ferromagnetic glasses in the Fe-Ni-P-B system [J]. Acta Mater, 2001, 49: 837−847.

[12] WILDE G, KLOSE S G, SOELLNER W, GORLER G P, JEROPOULOS K, WILLNECKER R. On the stability limits of the undercooled liquid state of Pd-Ni-P [J]. Mater Sci Eng A, 1997, 226: 434−438.

[13] SHEK C H, LIN G M. Dilatometric measurement and calculation of effective pair potentials for $Zr_{41}Ti_{14}Cu_{12.5}Ni_{10}Be_{22.5}$ bulk metallic glass [J]. Mater Lett, 2003, 57: 1229−1232.

[14] DONG C, WANG Q, QIANG J B, WANG Y M, JIANG N, HAN G, LI Y H, WU J, XIA J H. From clusters to phase diagrams: Composition rules of quasicrystals and bulk metallic glasses [J]. J Phys D: Appl Phys, 2007, 40: R273−R291.

[15] WANG W M, GEBERT A, ROTH S, KUEHN U, SCHULTZ L. Glass formability and fragility of $Fe_{61}Co_{9-x}Zr_8Mo_5W_xB_{17}$ (x=0 and 2) bulk metallic glassy alloys [J]. Intermetallics, 2008, 16: 267−272.

[16] LU Z P, LIU C T, THOMPSON J R, PORTER W D. Structural amorphous steels [J]. Phys Rev Lett, 2004, 92: 245503−1−4.

[17] ZHANG B, ZHAO D Q, PAN M X, WANG R J, WANG W H. Formation of cerium-based bulk metallic glasses [J]. Acta Mater, 2006, 54: 3025−3032.

[18] TURNBULL D. Under what conditions can a glass be formed [J]. Contemp Phys, 1969, 10: 473−488.

[19] WANG W H, PAN M X, ZHAO D Q, HU Y, BAI H Y. Enhancement of the soft magnetic properties of FeCoZrMoWB bulk metallic glass by microalloying [J]. J Phys Condens Matter, 2004, 16: 3719−3723.

[20] ECKERT J, KUBLER A, SCHULTZ L. Mechanically alloyed $Zr_{55}Al_{10}Cu_{30}Ni_5$ metallic glass composites containing nanocrystalline W particles [J]. J Appl Phys, 1999, 85: 7112−7119.

[21] FANG S S, XIAO X S, XIA L, LI W H, DONG Y D. Relationship between the widths of supercooled liquid regions and bond parameters of Mg-based bulk metallic [J]. J Non-Cryst Sol, 2003, 321: 120−125.

(Edited by YANG Bing)